Effects of multichance fission on mass yields at high energies

Dong-Ying Huo ⬤,[1] Zheng Wei ⬤,[1,2,3,*] Kang Wu ⬤,[1] Yi-Xuan Wang,[1] Chao Han,[1] Jun Ma,[1] Jun-Run Wang,[1,2,3] Yu Zhang,[1,2,3] and Ze-En Yao[1,2,3]

[1]*School of Nuclear Science and Technology, Lanzhou University, 730000 Lanzhou, China*
[2]*Engineering Research Center for Neutron Application Technology, Ministry of Education, Lanzhou University, 730000 Lanzhou, China*
[3]*MOE Frontiers Science Center for Rare Isotopes, Lanzhou University, Lanzhou 730000, China*

The mass distributions of fragment for neutron-induced ^{235,238}U, ^{237}Np, and ^{239}Pu fission were studied using the improved scission point model by considering the octupole deformation of the fragments over a wide range of incident neutron energies ($E_n = 10-50$ MeV). The multichance fission mechanism ensures that the mass distributions remain highly asymmetric even at high energy. We also investigated the role of octupole deformation of fragments in the multichance fission mechanism. The results obtained using the improved scission point model accurately replicated the experimental data. This model is expected to further our understanding of the fission process of actinides in the high excitation energy region.

I. INTRODUCTION

Since the discovery of the phenomenon of neutron-induced fission of uranium in 1938 [1,2], nuclear energy has been extensively studied for its application in power generation. One of the most crucial issues associated with the use of nuclear energy is the management of nuclear waste. Accelerator-driven systems (ADSs) are recognized by the international nuclear community as a powerful tool for transmutation minor actinides and long-lived fission products using high-energy spallation neutrons [3,4]. Therefore, it is crucial to understand the mechanism of fission at high excitation energies to evaluate neutron-induced fission data associated with the transmutation system.

The scission point model, as a typical statistical method, can calculate and reproduce mass distributions [5–12]. The potential at the scission point is determined by the liquid-drop (LD) energy and shell correction of the proton and neutron subsystems of the two nascent fragments and their interaction. As the excitation increases, the impact of the shell effect diminishes, and the symmetric distribution type becomes more dominant. It is possible to fit the experimental data with a single Gaussian provided if the excitation energy is sufficiently high to eliminate the shell effect. However, the asymmetric fission phenomenon was still observed in the high-energy region [13–16]. The key phenomenon in high-energy fission is the evaporation of neutrons before fission, resulting multichance fission (MCF), also known as fission after successive evaporation of neutrons. Neutron evaporation results in a considerable decrease in excitation energy, thus restoring the shell effect at low excitation energy. Asymmetric fission is the dominant mechanism for higher-order fission. The MCF mechanism is the only plausible explanation for asymmetry in mass distribution at high excitation energies. The Japanese group [13]

compared their fission product yields with theoretical results based on the three-dimensional Langevin model, clearly mentioning the effect of the MCF.

In the current experimental conditions, it is not possible to determine the number of neutron emissions before fission on an event-by-event basis. As a result, the observed fragments mass distribution is typically a combination of various fission chances. Therefore, the above conclusion cannot be experimentally verified with certainly at present. We have to develop theoretical approaches in order to study the effects of MCF on the basis of available experimental data.

The fission fragments will deform under strong interactions at the scission point. The scission point model [5–11] assumed that the shapes of most heavy nuclei are characterized by spherical and quadrupole deformation. In previous research [12], we improved the scission point model by considering the octupole deformations of the fission fragments. This advancement enables more accurate calculations of yields for neutron-induced fission of typical actinides. And we will investigate the effect of MCF on the mass distribution based on the improved scission point model.

This paper aims to demonstrate the current understanding of the fission process of actinides at higher excitation energy regions, where MCF effects are essential, by incorporating the MCF mechanism into the improved scission point model. The paper is organized as follows. Section II provides a brief overview of our model. The discussion is given on the results obtained by considering the MCF mechanism in Sec. III. Finally, Sec. IV presents a summary.

II. METHODS

The basic assumption of the scission point model is that statistical equilibrium is established at the scission where the observable characteristics of the fission process are formed. When the deformation is large enough, the parent nucleus

*Contact author: weizheng@lzu.edu.cn

undergoing fission splits into a pair of nearly touching coaxial daughter nuclei. For simplicity, we have adopted axial symmetry deformations (β_{2i}, β_{3i}), where the index i $(i = L, H)$ designates the light or heavy fragment.

The distribution of fission fragment is determined by the relative potential energy of a given fragmentation combination at the scission point. The potential energy includes the binding energy of the light (L) and heavy (H) fragments with the mass numbers A_L (A_H) and charge numbers Z_L (Z_H), as well as the Coulomb potential and nuclear potential between the two fragments. The potential energy U at the scission point as a function of the deformations and the internuclear distance R between fragments is described as

$$
\begin{aligned}
U(A_i, Z_i, \beta_i, R) &= B(A_L, Z_L, \beta_{2L}, \beta_{3L}, E_L^*) \\
&\quad + B(A_H, Z_H, \beta_{2H}, \beta_{3H}, E_H^*) \\
&\quad - B(A, Z, \beta_2, \beta_3, E^*) \\
&\quad + V_C(A_i, Z_i, \beta_{2i}, \beta_{3i}, R) \\
&\quad + V_N(A_i, Z_i, \beta_{2i}, \beta_{3i}, R),
\end{aligned}
\tag{1}
$$

where $A = A_L + A_H$ ($Z = Z_L + Z_H$) is the mass (charge) number of the compound nucleus. The deformation parameters are denoted by $\beta_{\lambda i}$, where ($\lambda = 2, 3; i = L, H$) represent quadrupole and octupole deformations of the light and heavy fragments, respectively. The R corresponds to the $R_m = R_L + R_H + 0.5$ fm at which the potential pocket takes the minimum value of interaction potential [17].

The binding energies $B(A_i, Z_i, \beta_{2i}, \beta_{3i}, E_i^*)$ as a function of quadrupole β_{2i} and octupole β_{3i} deformations are calculated by using the macroscopic microscopic method [18,19]. The binding energy of each fragment consists of the liquid drop energy U^{LD}, the shell correction energy δU^{shell}.

The impact of excitation energy on mass distributions arises from the complex interplay between the macroscopic liquid-drop energies and microscopic shell corrections at scission. The shell correction is calculated using the traditional Strutinsky procedure, which involves summing the shell energies of protons and neutrons [20]. The damping of the shell correction with excitation energy is introduced as

$$
\begin{aligned}
\delta U^{shell}&(A_i, Z_i, \beta_{2i}, \beta_{3i}, E_i^*) \\
&= \delta U^{shell}(A_i, Z_i, \beta_{2i}, \beta_{3i}, E_i^* = 0) * S(E_i^*),
\end{aligned}
\tag{2}
$$

$$
S(E) = \exp(-E_i^*/E_D),
\tag{3}
$$

where $E_D = 20$ MeV [13] is the damping constant, meaning the speed of washing out the shell correction against the excitation energy.

The interaction potential consists of the Coulomb potential V_C and nuclear potential V_N. The Coulomb interaction can be calculated by using Wong's formula [21] and the nuclear potential [17] is expressed as the double-folding form.

The relative formation probability w with fragments of certain charge numbers, mass numbers, and deformations can be described as

$$
w(A_i, Z_i, \beta_{2i}, \beta_{3i}, E^*) = \exp\left(-\frac{U(A_i, Z_i, \beta_{2i}, \beta_{3i}, R_m)}{T}\right).
\tag{4}
$$

The temperature is calculated as $T = \sqrt{E^*/a}$, where $a = A/12$ MeV^{-1} [17] is the level density parameter in the Fermi-gas model. The excitation energy at scission is the initial excitation E_{CN}^* ($E_{CN}^* = E_n + Q$) minus the potential energy $U(A_i, Z_i, \beta_{2i}, \beta_{3i}, R_m)$, which is expressed as

$$
E^*(A_i, Z_i, \beta_{2i}, \beta_{3i}, R_m) = E_{CN}^* - U(A_i, Z_i, \beta_{2i}, \beta_{3i}, R_m).
\tag{5}
$$

Here, the E_n is the neutron kinetic energy and Q is the reaction energy. Following neutron evaporation, the excitation energy E^* decreases due to the emission of neutrons. The initial compound nucleus A_{CN} can decay through first chance or single neutron emission, resulting in a decrease in the initial excitation energy. The subsequent nucleus can decay through second fission or again neutron evaporation to $A_{CN}-2$. The energy removed from the initial excitation energy E^* due to neutron evaporation is the sum of the kinetic energy and the binding energy of the neutrons. The excitation energy is recalculated for each neutron that is evaporated, which can be expressed as

$$
E_{(n,xnf)}^* = E_{CN}^* - x(B_n^{(n,xnf)} + \bar{\varepsilon}),
\tag{6}
$$

where $\bar{\varepsilon}$ is the mean neutron kinetic energy, which is calculated using the GEF code [22,23]. The $B_n^{(n,xnf)}$ is the binding energy of the neutrons [24] and the x is the number of evaporating neutrons.

β_{2i} and β_{3i} should be integrated over to acquire the mass-charge distribution of the fragment yields of each chance, which is express as

$$
\begin{aligned}
Y_{(n,xnf)}(A_i, Z_i, E_{(n,xnf)}^*) &= \int d\beta_{2L} d\beta_{2H} d\beta_{3L} d\beta_{3H} w \\
&\quad \times (A_i, Z_i, \beta_{2i}, \beta_{3i}, E_{(n,xnf)}^*).
\end{aligned}
\tag{7}
$$

The total yields are the sum of the weights of each fission chance,

$$
Y_{tot}(A_i, Z_i, E^*) = \sum_{x=1} w_x Y_{(n,xnf)}(A_i, Z_i, E_{(n,xnf)}^*).
\tag{8}
$$

The weight (probability) w_x of each fission chance is determined using the statistical model code GEF [23]. Eventually, the mass distributions of the fission fragments should be normalized to 200% by definition, with N_0 as the normalization constant. The mass distributions can be evolved into

$$
Y_{tot}(A_i, E^*) = N_0 \sum_{Z_i} Y_{tot}(A_i, Z_i, E^*).
\tag{9}
$$

III. RESULTS AND DISCUSSION

Figure 1 shows the minimum potential energy and corresponding mass yields for neutron-induced fission of ^{238}U as a function of mass number. At the low excitation ($E_n = 10$ MeV), the minimum potential energy exhibits a clear double-humped shape. At the high-energy fission ($E_n = 45$ MeV), the minimum potential energy takes on an almost single-Gaussian-like shape, which leads to an increase in the probability of symmetric fission and a decrease of the peak to valley as the excitation energy increases in neutron-induced
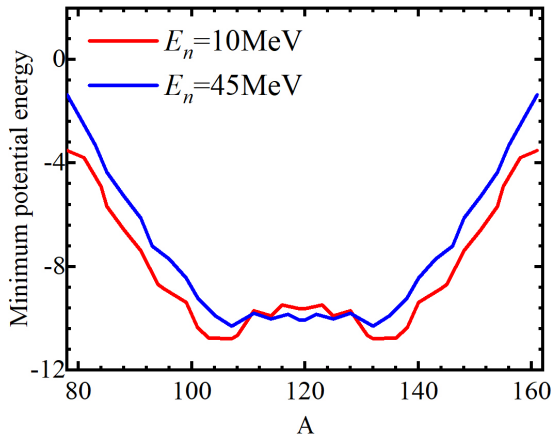
FIG. 1. The minimum potential energy for neutron-induced fission of ^{238}U at $E_n = 10$ MeV and $E_n = 45$ MeV as a function of the mass number.

fission of ^{238}U. The result demonstrates a transition to symmetric type fission.

As the excitation energy increases, two competing processes are expected: an increase in symmetric fission probability, as previously demonstrated, and the occurrence of multichance fission. The effect of MCF on the mass distributions is exemplified in Fig. 2, which shows the case of neutron-induced ^{238}U fission with an incident energy of 32.5 MeV. By ignoring MCF, it is assumed that the calculated mass distribution is solely due to the direct fission of initial excitation energy, without any neutron evaporation in the compound nucleus. The resulting distribution is shown as the black line in Fig. 2. However, this assumption leads to a significantly smaller peak-valley ratio compared to the experimental data (black symbols with error bars). Additionally, the peak position $A_L \approx 106$ ($A_H \approx 133$) deviates from the measured value $A_L \approx 100$ ($A_H \approx 139$). Then MCF has been taken into account in the model. The initial compound nucleus ^{239}U is highly excited and can either decay through first fission or neutron emission, resulting in the production of ^{238}U at
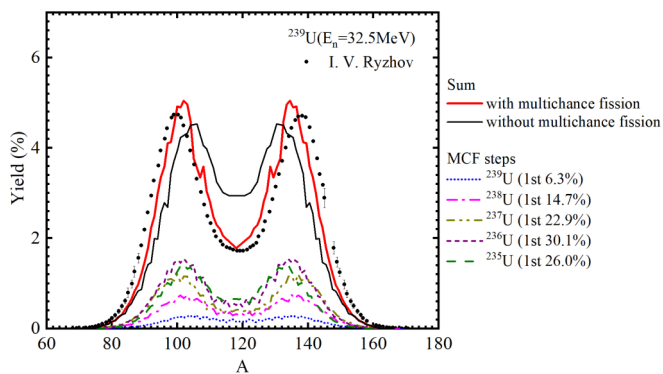

FIG. 2. The calculated mass distributions without (black curve) and with (red curve) MCF for neutron-induced ^{238}U fission with incident neutron energies of 32.5 MeV are compared with the experimental data (black symbols with error bars) from Ref. [25]. The calculated mass distributions for all the fission chances (dashed curves with different colors) are shown.
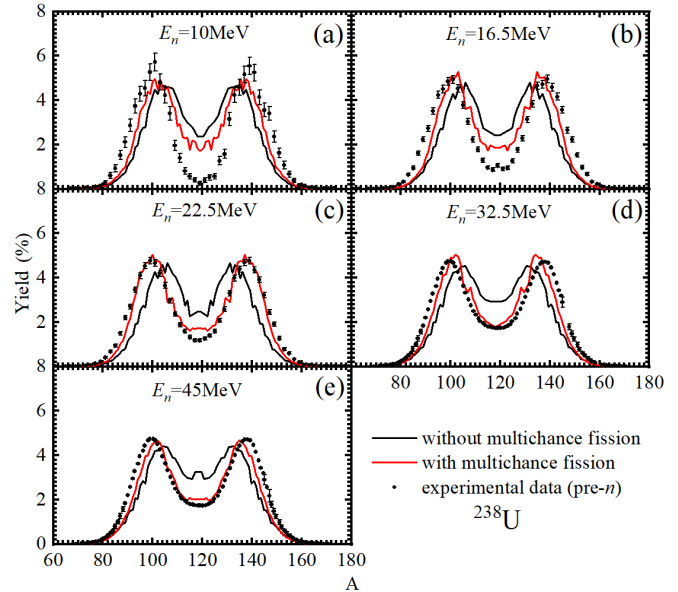

FIG. 3. The calculated mass distributions without (black curve) and with (red curve) MCF for fission of ^{238}U by neutron induced in the range of incident neutron energies $E^* = 10 - 45$ MeV are compared with the experimental data (black symbols with error bars) from Ref. [25].

a lower excitation state. The ^{238}U nucleus can then undergo further decay through second fission or neutron evaporation. The multichance fission will not occur until the excitation falls below the fission barrier. The excitation energy of the residual nucleus after each neutron emission can be calculated based on the neutron binding energy and average energy of the emitted neutron. The potential energy surface of the residual nucleus was also recalculated at each step using the scission point model. The probability of each fission chance and the average energy of the emitted neutron were determined using the GEF code. The dashed curves in different colors show the calculated mass distributions for all the fission chances, while the red curve represents the sum of all mass distributions. The results reproduce the peak position of the experimental data [25], but with a slightly larger peak-valley ratio. The MCF mechanism ensures that the compound nucleus remains highly characterized by an asymmetric distribution even at high energy. This asymmetry mainly arises from third, fourth, and fifth chance fissions ($^{237, 236, 235}$U) at lower energy.

To verify the model description, Figs. 3–5 show the calculated mass distributions for neutron-induced fission of ^{235,238}U, ^{237}Np, and ^{239}Pu with MCF mechanism (red curves). The peak-valley ratio of all elements (^{235,238}U, ^{237}Np, and ^{239}Pu) decreases as the excitation energy increases. The calculation with MCF reproduces experimental data [26–30] well in the range of incident neutron energies $E^* = 10 - 50$ MeV, in contrast to the results without MCF (black curves). The MCF mechanism introduces higher shell-damping energy, which leads to a still highly asymmetric distribution even at high energy. These results suggest that the asymmetry in the high-energy region should not be interpreted as a function of shell effects in the initial compound nucleus.
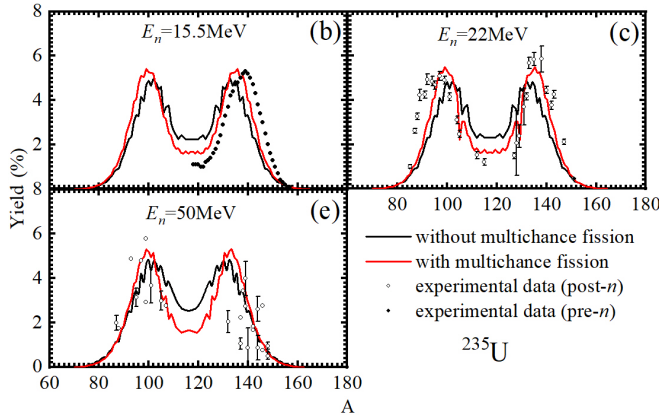
FIG. 4. The calculated mass distributions without (black curve) and with (red curve) MCF for fission of ^{235}U by neutron induced in the range of incident neutron energies $E^* = 15.5 - 50$ MeV are compared with the experimental data (black symbols with error bars) from Refs. [26–28].

In order to illustrate the contribution of octupole deformation in the MCF mechanism, we have calculated the mass distributions of ^{238}U(n, f) at $\beta_3 = 0$ (blue dashes line) and without deformation restriction (β_{2i} and β_{3i} change from 0.0 to 0.5 in steps of 0.05) (red solid line), which are compared with experimental data at the incident neutron energy of 10 MeV [25] in Fig. 6. The calculated mass distributions without deformation restriction exhibit a peak position in good agreement with experimental data. The octupole deformation of fission fragments exerts a significant influence, especially in peak position and wide distribution, on the mass distribution of ^{238}U at low excitation energies, which is produced by the evaporation of neutrons of compound nucleus ^{239}U. Since the light fragments also have octupole deformation and this can reduce corresponding potential-energy surface, which results in a larger yields and wider distribution of the corresponding light fragments not underestimates the mass yields for $A_L < 94$ [12]. The MCF mechanism ensures that the compound nucleus remains highly characterized by an asymmetric distribution even at high energy. This asymmetry is primarily attributable to the lower-energy fission of the
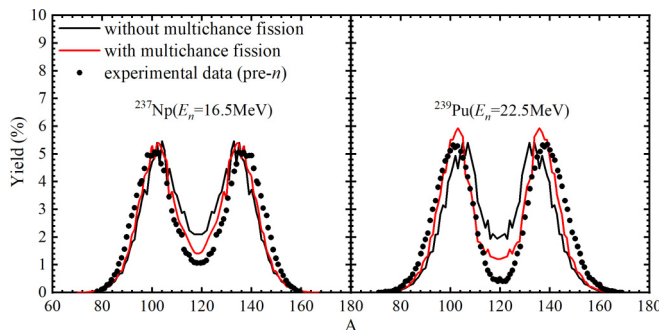

FIG. 5. The calculated mass distributions without (black curve) and with (red curve) MCF for fission of ^{237}Np and ^{239}Pu are compared with the experimental data (black symbols with error bars) from Refs. [29,30].
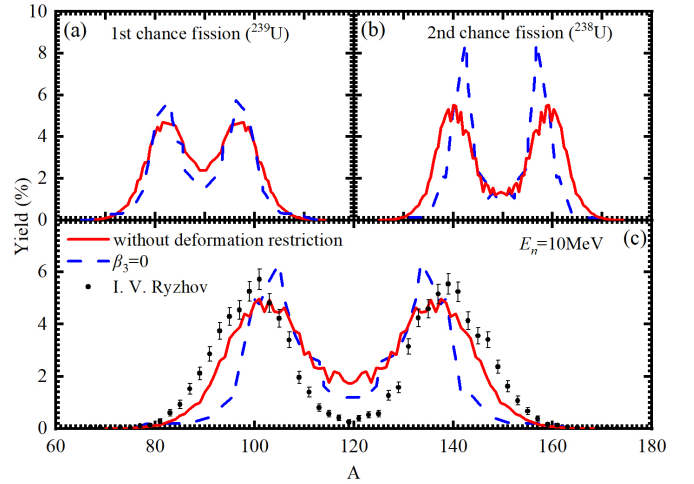

FIG. 6. The calculated mass distributions of sum (c) and the first (a) and second (b) chance fission at $\beta_3 = 0$ (blue dashed line) and without deformation restriction (red solid line) for neutron-induced ^{238}U fission with incident neutron energy of 10 MeV are compared with the experimental data [25] (black symbols with error bars).

compound nucleus subsequent to the evaporation of neutrons. The consideration of octupole deformation of fission fragments ensures the precision of low-energy fission calculations.

IV. CONCLUSION

Under the current experimental conditions, it is not possible to distinguish between mass yields originating from the initial compound nucleus and those resulting from other isotopes with lower excitation via a chain of multichance fission. The observed mass distributions are typically a combination of various fission chances. Unfortunately, there is no suitable model to calculate mass distribution with sufficient accuracy. As a result, the impact of MCF on the mass distribution is limited.

This work presents the mass distributions of actinides fission in the high-energy region, calculating using the improved scission point model considering the MCF mechanism. Concurrently, the introduction of octupole deformation of the fission fragments ensures the accuracy of the yields for each fission chance. The model offers a better explanation of the experimental data and the relative contributions of symmetric and asymmetric modes at different excitation energies. The results exhibit significant asymmetry, which is attributed to the fission of less excited lighter isotopes produced through a chain of MCF. The present study confirms the existence of MCF as the mechanism responsible for the asymmetry of the mass distributions at high excitation energies.

The scission point model is improved by considering MCF, which shows a significant advancement in calculating yields of neutron-induced typical actinides fission in the high-energy region. The role of MCF is expected to further our understanding of the fission process.

ACKNOWLEDGMENTS

[1] O. Hahn and F. Strassman, Naturwissenschaften **27**, 11 (1939).

[2] L. Meitner and O. R. Frisch, Nature (London) **143**, 239 (1939).

[3] T. Mukaiyama, T. Takizuka, M. Mizumoto, Y. Ikeda, T. Ogawa, A. Hasegawa, H. Takada, and H. Takano, Prog. Nucl. Energy **38**, 107 (2001).

[4] A. Brolly and P. Vértes, Acta Phys. Hung. A **19**, 263 (2004).

[5] B. D. Wilkins, E. P. Steinberg, and R. R. Chasman, Phys. Rev. C **14**, 1832 (1976).

[6] H. Pasca, A. V. Andreev, G. G. Adamian, and N. V. Antonenko, Phys. Rev. C **104**, 014604 (2021).

[7] H. Pasca, A. V. Andreev, G. G. Adamian, and N. V. Antonenko, Phys. Rev. C **101**, 064604 (2020).

[8] H. Pasca, A. V. Andreev, G. G. Adamian, and N. V. Antonenko, Phys. Rev. C **99**, 064611 (2019).

[9] J.-F. Lemaître, S. Panebianco, J. L. Sida, S. Hilaire, and S. Heinrich, Phys. Rev. C **92**, 034617 (2015).

[10] J.-F. Lemaître, S. Goriely, S. Hilaire, and J. L. Sida, Phys. Rev. C **99**, 034612 (2019).

[11] D. Y. Huo, X. Yang, C. Han, C. Q. Liu, K. Wu, X. Y. Liu, C. Huang, Q. Xie, Y. He, X. J. Bao, Z. E. Yao, Y. Zhang, J. R. Wang, X. D. Su, and Z. Wei, Chin. Phys. C **45**, 114104 (2021).

[12] D. Y. Huo, Z. Wei, K. Wu, C. Han, Y. N. Han, Y. X. Wang, P. Q. Zhang, Y. He, X. J. Bao, Z. Y. Deng, and Z. E. Yao, Phys. Rev. C **108**, 024608 (2023).

[13] K. Hirose, K. Nishio, S. Tanaka, R. Leguillon, H. Makii, I. Nishinaka, R. Orlandi, K. Tsukada, J. Smallcombe, M. J. Vermeulen, S. Chiba, Y. Aritomo, T. Ohtsuki, K. Nakano, S. Araki, Y. Watanabe, R. Tatsuzawa, N. Takaki, N. Tamura, S. Goto *et al.*, Phys. Rev. Lett. **119**, 222501 (2017).

[14] M. Caamaño, O. Delaune, F. Farget, X. Derkx, K.-H. Schmidt, L. Audouin, C.-O. Bacri, G. Barreau, J. Benlliure, E. Casarejos *et al.*, Phys. Rev. C **88**, 024605 (2013).

[15] S. Santra, A. Pal, D. Chattopadhyay, A. Kundu, P. C. Rout, Ramandeep Gandhi, A. Baishya, T. Santhosh, K. Ramachandran, R. Tripathi, B. J. Roy, T. N. Nag, G. Mohanto, S. De, B. K. Nayak, and S. Kailas, Phys. Rev. C **107**, L061601 (2023).

[16] B. B. Back, A. C. Shotter, T. J. M. Symons, A. Bice, C. K. Gelbke, T. C. Awes, and D. K. Scott, Phys. Rev. C **23**, 1105 (1981).

[17] H. Pasca, A. V. Andreev, G. G. Adamian, N. V. Antonenko, and Y. Kim, Phys. Rev. C **93**, 054602 (2016).

[18] N. Wang, M. Liu, and X. Wu, Phys. Rev. C **81**, 044322 (2010).

[19] X. H. Ruan, J. T. Hu, and T. Rong, J. Phys. G: Nucl. Part. Phys. **46**, 125108 (2019).

[20] V. M. Strutinsky and F. A. Ivanjuk, Nucl. Phys. A **255**, 405 (1975).

[21] C. Y. Wong, Phys. Rev. Lett. **31**, 766 (1973).

[22] K.-H. Schmidt, B. Jurado, C. Amouroux, and C. Schmitt, Nucl. Data Sheets **131**, 107 (2016).

[23] B. Jurado and K. H. Schmidt, Computer code GEF, version 1.2, 2020, http://www.cenbg.in2p3.fr/GEF.

[24] P. Moller, J. R. Nix, W. D. Myers, and W. J. Swiatecki, At. Data Nucl. Data Tables **59**, 185 (1995).

[25] I. V. Ryzhov, S. G. Yavshits, G. A. Tutin, N. V. Kovalev, A. V. Saulski, N. A. Kudryashev, M. S. Onegin, L. A. Vaishnene, Y. A. Gavrikov, O. T. Grudzevich, V. D. Simutkin, S. Pomp, J. Blomgren, M. Osterlund, P. Andersson, R. Bevilacqua, J. P. Meulders, and R. Prieels, Phys. Rev. C **83**, 054603 (2011).

[26] P. P. D'yachenko, B. D. Kuz'minov, and M. Z. Tarasko, Yad. Fiz. **8**, 286 (1968).

[27] J. Feng, Y. H. Liu, Y. Yang, J. Bao, Z. Li, B. J. Qi, H. Q. Tang, Z. Y. Zhou, A. Z. Cui, X. C. Ruan, H. Q. Sun, S. D. Zhang, and J. R. Guo, China Inst. of Atomic Energy **053**, 4 (2001).

[28] W. Younes, J. A. Becker, L. A. Bernstein, P. E. Garrett, C. A. McGrath, D. P. McNabb, R. O. Nelson, G. D. Johns, W. S. Wilburn, and D. M. Drake, Phys. Rev. C **64**, 054613 (2001).

[29] D. M. Gorodisskiy, K. V. Kovalchuk, S. I. Mulgin, A. Ya. Rusanov, and S. V. Zhdanov, Ann. Nucl. Energy **35**, 238 (2008).

[30] H. Thierens, A. De Clercq, E. Jacobs, D. De Frenne, P. D'hondt, P. De Gelder, and A. J. Deruytter, Phys. Rev. C **23**, 2104 (1981).